Lithium Mobility in $Li_{1.2}Ti_{1.8}R_{0.2}(PO_4)_3$ Compounds (R = Al, Ga, Sc, In) as Followed by NMR and Impedance Spectroscopy

K. Arbi,[†,‡] M. G. Lazarraga,[†] D. Ben Hassen Chehimi,[‡] M. Ayadi-Trabelsi,[‡] J. M. Rojo,[†] and J. Sanz*[,†]

Instituto de Ciencia de Materiales de Madrid (ICMM), Consejo Superior de Investigaciónes Científicas (CSIC), Cantoblanco, 28049 Madrid, Spain, and Laboratoire PCM, Faculté de Sciences de Bizerte, Zarzouna 7021, Tunisia

Received June 4, 2003. Revised Manuscript Received October 16, 2003

Composition and lithium mobility have been analyzed in $Li_{1+x}Ti^{4+}_{2-x}R^{3+}_x(PO_4)_3$ compounds ($x = 0.2$ and $R^{3+} = Al^{3+}$, Ga^{3+}, Sc^{3+}, and In^{3+}) by NMR and impedance spectroscopy. All of the compounds display the rhombohedral symmetry, and in all cases the trivalent cations are incorporated into the NASICON framework. From the analysis of the quadrupole constant (C_Q) and spin−spin relaxation rate (T_2^{-1}) deduced from ^{7}Li NMR spectra of $Li_{1.2}Ti_{1.8}Al_{0.2}(PO_4)_3$, two regimes associated with local and long-range motions of lithium have been identified. From the analysis of the spin-lattice relaxation rate (T_1^{-1}) as a function of reciprocal temperature, the residence times of lithium at structural sites have been estimated and their dependence on temperature have been analyzed. Differences in activation energy deduced from NMR (0.22 eV) and conductivity (0.28 eV) measurements are discussed in terms of correlations in lithium motion that seem to decrease at increasing temperature.

Introduction

NASICON-type materials with formula $LM_2(PO_4)_3$ (L = Li, Na and M = Ge, Ti, Sn, Hf, and Zr) are of increasing interest because of their possible application as solid electrolytes in lithium batteries, sensors, and others electrochemical devices.[1−3] The usual structure of these compounds is rhombohedral, space group $R\bar{3}c$, but in some particular cases they also show a low-temperature phase of lower symmetry.[4−10] In both phases the framework is built up by $M_2(PO_4)_3$ units in which two MO_6 octahedra and three PO_4 tetrahedra share oxygen atoms (Figure 1). In the rhombohedral sodium phases, Na^+ cations are placed at two structural sites: (i) M_1 sites surrounded by six oxygen atoms and located at inversion centers, and (ii) M_2 sites with an irregular 10-fold oxygen coordination and disposed symmetrically around ternary axes. Both sites are arranged in an alternating way along the conducting channels. In rhombohedral lithium phases, such as $LiGe_2(PO_4)_3$ and $LiTi_2(PO_4)_3$, the preferential occupancy of M_1 sites by lithium has been pointed out from neutron diffraction (ND) experiments.[11−12] When the size of the tetravalent cation increases (e.g., M = Sn, Hf, Zr), a low-

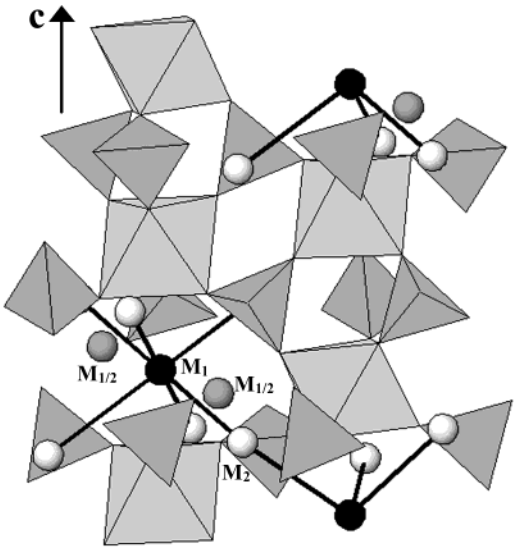

Figure 1. View of the NASICON framework showing the $M_2(PO_4)_3$ units and structural sites occupied by alkaline cations (M_1, $M_{1/2}$, and M_2).

* To whom correspondence should be addressed. E-mail: jsanz@icmm.csic.es.
† Instituto de Ciencia de Materiales de Madrid.
‡ Laboratoire PCM, Faculté de Sciences de Bizerte.

(1) Julien, C.; Nazri, G.-A. *Solid State Batteries: Materials Design and Optimization*; Kluwer Academic Publishers: Boston, MA, 1994.
(2) Collin, G.; Boilot, J. P. In *Superionic Solids and Solid Electrolytes*; Laskar, A. L., Chandra, S., Eds.; Academic Press: Boston, MA, 1989.
(3) Velasco, G. *Solid State Ionics* **1983**, *9*−*10*, 783−792.
(4) Hong, H. Y.-P. *Mater. Res. Bull.* **1976**, *11*, 173−182.
(5) Goodenough, J. B.; Hong, H. Y.-P.; Kafalas, J. A. *Mater. Res. Bull.* **1976**, *11*, 203−220.
(6) Hagman, L.; Kierkegaard, P. *Act. Chem. Scand.* **1968**, *22*, 1822.
(7) Sudreau, F.; Petit, D.; Boilot, J. P. *J. Solid State Chem.* **1989**, *83*, 78−90.
(8) Morin, E.; Angenault, J.; Couturier, J. C.; Quarton, M.; He, H.; Klinowski, J. *Eur. J. Solid State Inorg. Chem.* **1997**, *34*, 947−958.
(9) Losilla, E. R.; Aranda, M. A. G.; Martinez-Lara, M.; Bruque, S. *Chem. Mater.* **1997**, *9*, 1678−1685.
(10) Catti, M.; Stramare, S.; Ibberson, R. *Solid State Ionics* **1999**, *123*, 173−180.
(11) Alami, M.; Brochu, R.; Soubeyroux, J. L.; Graverau, P.; le Flem, G.; Hagenmuller, P. *Solid State Chem.* **1991**, *90*, 185−193.
(12) Tran Qui, D.; Hamdoune, S.; Soubeyroux, J. L.; Prince, E. *J. Solid State Chem.* **1988**, *72*, 309−315.

10.1021/cm030422i CCC: $27.50
Published on Web 12/25/2003

temperature triclinic phase has also been detected. In this phase, Li^+ ions are placed at the midway $M_{1/2}$ positions between M_1 and M_2 sites in a 4-fold oxygen coordination[8−10] (Figure 1).

In titanium-based NASICON-type materials of $Li_{1+x}Ti_{2-x}R_x(PO_4)_3$ composition, the Li^+ ion conductivity of the rhombohedral phase is greatly enhanced as Ti^{4+} is partially replaced by trivalent cations such as Al, Ga, Sc, and In.[13] In these samples, the charge deficit is compensated by the incorporation of additional lithium in the structure. The maximum conductivity (10^{-2}−10^{-3} Ω^{-1} cm^{-1}) was found for the composition $x \approx 0.3$. In the $Li_{1+x}Ti_{2-x}Al_x(PO_4)_3$ series, a decrease in the overall conductivity was observed for $x > 0.3$, this decrease was attributed to the formation of nonconducting phases at the grain boundaries.[14] In the $Li_{1+x}Ti_{2-x}In_x(PO_4)_3$ series, the samples with $x > 0.3$ showed phases with structure different from the NASICON structure; these phases exhibited Li^+ conductivity considerably lower than that of the NASICON-type compounds.[15−18]

In this work, rhombohedral $Li_{1+x}Ti_{2-x}R_x(PO_4)_3$ samples ($x = 0.2$ and $R^{3+} = Al^{3+}$, Ga^{3+}, Sc^{3+}, In^{3+}, and Y^{3+}) have been prepared, and the unit-cell dimensions have been deduced from X-ray diffraction data. Distribution of octahedral R^{3+} cations has been followed by ^{31}P MAS NMR technique, and occupancy of lithium sites has been studied by ^7Li MAS NMR technique. The NMR and impedance techniques have been used to analyze the local and long-range motion of Li^+ ions, respectively. From the results obtained with both techniques, lithium hopping mechanisms have been analyzed.

Experimental Section

Samples were prepared by heating stoichiometric mixtures of Li_2CO_3 (≥99%), TiO_2 (99%), Al_2O_3 (99.99%), Ga_2O_3 (99.99%), Sc_2O_3 (99.999%), In_2O_3 (99.99%), Y_2O_3 (99.98%), and $(NH_4)_2HPO_4$ (≥99%). The reagents were previously heated at 120 °C for 10 h to remove the adsorbed water. Then they were mixed and heated in a platinum crucible at 180, 300, 500, 700, 800, 900, and 950 °C. After each treatment, the mixture was ground in an agate mortar and checked by X-ray diffraction. The samples were considered as single phases when typical X-ray peaks of the reagents and/or intermediate compounds such as pyrophosphates were not detected.

X-ray diffraction patterns were recorded at room temperature with Cu Kα_1 radiation ($\lambda = 1.5405981$ Å) in a PW-1710 Phillips diffractometer equipped with a graphite monochromator. Data were taken in the $10 \le 2\theta \le 70°$ range with 0.02° per step, counting for 0.5 s at each step. A small amount of Si (NIST, $a = 5.430940$ Å) was mixed with prepared samples to get an accurate determination of the peak positions in XRD patterns.

Two-probe impedance measurements were carried out with a 1260 Solartron impedance/gain phase analyzer. The frequency range used was 5−10^6 Hz. Measurements were made on cylindrical pellets of 13 mm diameter and 1−2 mm thickness. Pellets were compacted by cold pressing at 3 MPa, then they were sintered at 1000 °C for 24 h. Gold was used as electrode. Impedance measurements were carried out in the temperature range 150−300 K in an Oxford Cryostat. All measurements were done under a dried nitrogen atmosphere.

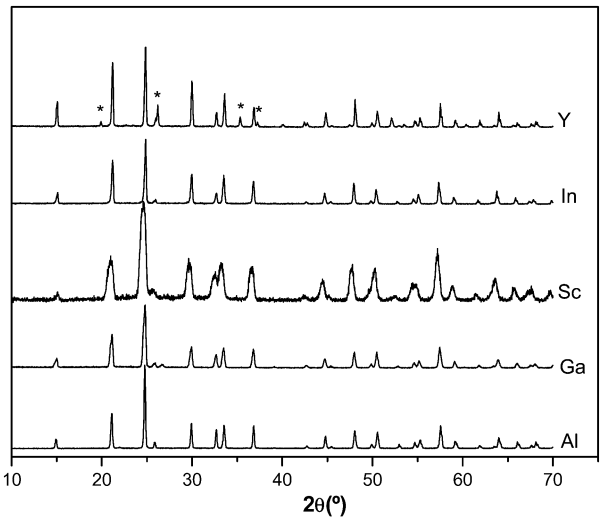

Figure 2. X-ray diffraction patterns of $Li_{1+x}Ti^{4+}_{2-x}R^{3+}_x(PO_4)_3$ ($R^{3+} = Al^{3+}$, Ga^{3+}, Sc^{3+}, In^{3+}, and Y^{3+}) recorded at room temperature. Peaks marked by asterisks (*) correspond to $Li_3Y_2(PO_4)_3$.

^7Li and ^{31}P MAS NMR spectra were recorded at room temperature in a MSL-400 Bruker spectrometer (9.4 T). The frequencies used for ^7Li and ^{31}P were 155.50 and 161.97 MHz, respectively. Samples were spun at 4 and 10 kHz during ^7Li and ^{31}P signal recording. Spectra were obtained after $\pi/2$ pulse irradiation (∼4 μs) with a recycling time of 10 s for lithium and 5 s for phosphorus. The number of scans was in the range of 40−800. ^7Li and ^{31}P chemical shift values were given relative to 1 M LiCl and 85% H_3PO_4 aqueous solutions. The fitting of the NMR spectra was undertaken with the Bruker WINFIT software package.[19] This program allows determination of the position, line width, and intensity of the NMR components with a nonlinear least-squares iterative method; however, quadrupole (C_Q) and asymmetry (η) parameters had to be deduced with a trial and error procedure. For quantitative purposes, the sum of integrated intensities of the spinning sidebands associated with each component was determined. ^7Li spin−lattice relaxation times (T_1) of the $Li_{1.2}Ti_{1.8}Al_{0.2}(PO_4)_3$ sample were measured at 11 MHz in a SXP 4/100 spectrometer. The T_1^{-1} values were obtained with the $\pi - \tau - \pi/2$ sequence in the range 100−450 K. Reciprocal spin−spin relaxation times values (T_2^{-1}) were calculated from the full width at half-height (fwhh) of NMR lines. In the case of Gaussian lines T_2^{-1} was calculated as 0.6π times the fwhh; in the case of Lorenzian lines, T_2^{-1} was calculated as π times the fwhh.

Results

X-ray Diffraction. The XRD patterns of $Li_{1.2}Ti_{1.8}R_{0.2}(PO_4)_3$ ($R^{3+} = Al^{3+}$, Ga^{3+}, Sc^{3+}, and In^{3+}) recorded at room temperature are given in Figure 2. In most cases, the peaks are narrow and correspond to the rhombohedral ($R\bar{3}c$) NASICON phase. However, in the case of the scandium sample the peaks are considerably broadened, indicating a lower crystallinity. When Ti^{4+} is partially substituted by smaller R^{3+} cations such as Al^{3+}, a decrease in the hexagonal cell parameters of the rhombohedral phase is observed (Table 1). In contrast,

(13) Aono, H.; Sugimoto, E.; Sadaoka, Y.; Imanaka, N.; Adachi, G.-Y. *J. Electrochem. Soc.* **1990**, *137*, 1023−1027.
(14) Arbi, K.; Mandal, S.; Rojo, J. M.; Sanz, J. *Chem. Mater.* **2002**, *14*, 1091−1097.
(15) Hamdoune, S.; Tranqui, D.; Schouler, E. J. L. *Solid State Ionics* **1986**, *18−19*, 587−591.
(16) Hamdoune, S.; Gondrand, M.; Tran Qui, D. *Mater. Res. Bull.* **1986**, *21*, 237−242.
(17) Shi-Chun, L.; Zu-Ziang, L. *Solid State Ionics* **1983**, *9−10*, 835−838.
(18) Pronin, I. S.; Sigaryov, S. E.; Vashman, A. A. *Solid State Ionics* **1990**, *38*, 9−24.
(19) Massiot, D. WINFIT; Bruker-Franzen Analytik GmbH.: Bremen, Germany, 1993.

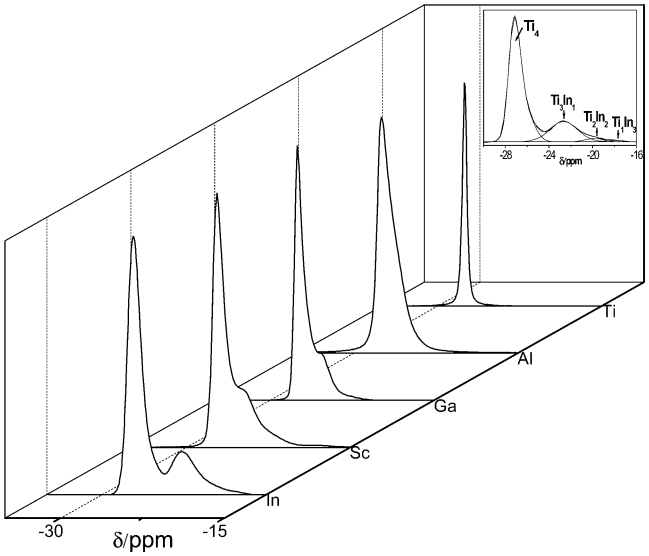

Figure 3. ^{31}P MAS NMR spectra of $Li_{1+x}Ti^{4+}_{2-x}R^{3+}_x(PO_4)_3$ series. Deconvolution of NMR signals on four components associated with $P(OTi)_4$, $P(OTi)_3(OR)_1$, $P(OTi)_2(OR)_2$, $P(OTi)_1(OR)_3$ environments is illustrated as an inset for the In sample.

Table 1. Hexagonal Unit Cell Parameters of the $Li_{1.2}Ti_{1.8}^{4+}R_{0.2}^{3+}(PO_4)_3$ Series; Ionic Radii of Trivalent Cations Are Also Included

R^{3+}	ionic radii of R^{3+} (Å)	*a* (Å)	*c* (Å)
Al^{3+}	0.53	8.501	20.770
Ga^{3+}	0.62	8.515	20.884
Sc^{3+}	0.74	8.533	20.986
In^{3+}	0.80	8.550	20.960

when Ti^{4+} is substituted by R^{3+} cations with larger ionic radii (Ga, Sc, In) an increase in the hexagonal lattice parameters is observed. We have also analyzed the sample with $R^{3+} = Y^{3+}$; in this case the XRD pattern is formed by intense peaks that are characteristic of the rhombohedral NASICON phase and by low-intensity peaks, marked with asterisks, that correspond to the secondary segregated $Li_3Y_2(PO_4)_3$ phase. From the intense XRD peaks we have deduced the hexagonal cell parameters (a = 8.516 Å and c = 20.848 Å) that are nearly the same as those of the undoped $LiTi_2(PO_4)_3$ sample (a = 8.513 Å and c = 20.820 Å). This fact indicates that Y^{3+} is not incorporated into the NASICON framework.

NMR

^{31}P NMR Signal. $^{31}P(I = {}^1/_2)$ MAS NMR spectra of the analyzed samples are shown in Figure 3. The ^{31}P spectrum of undoped $LiTi_2(PO_4)_3$ displays a single narrow line at −27.5 ppm. When the Ti^{4+} is substituted by trivalent R^{3+} cations, the ^{31}P NMR line becomes asymmetric and new low-intensity components at more positive chemical shifts are detected (Table 2). We observe that the separation between these components increases as the difference between ionic radii of Ti^{4+} and R^{3+} cations increases. In general, cations with small radii pull the electron density away from oxygen atoms, leaving phosphorus atoms more positively charged. But bigger atoms with lower polarizing strength produce the opposite effect, shifting ^{31}P NMR components toward lower shielding values.[20]

For the random distribution of R^{3+} and Ti^{4+} cations, five environments for phosphorus can be formed: $P(OTi)_4$, $P(OTi)_3(OR)_1$, $P(OTi)_2(OR)_2$, $P(OTi)_1(OR)_3$, and $P(OR)_4$. Taking into account that the chemical shift becomes more positive when Ti^{4+} is replaced by R^{3+} cations, the four detected components have been ascribed to $P(OTi)_4$, $P(OTi)_3(OR)_1$, $P(OTi)_2(OR)_2$, and $P(OTi)_1(OR)_3$.

From the integrated intensities of ^{31}P NMR components, the chemical composition of the samples has been estimated. In particular, Ti^{4+}/R^{3+} ratios have been calculated according to the expression[21]

$$\frac{Ti^{4+}}{R^{3+}} = \frac{4I_0 + 3I_1 + 2I_2 + I_3}{I_1 + 2I_2 + 3I_3 + 4I_4} \quad (1)$$

where I_n (n = 0, 1, 2, 3, 4) represents the intensity of the bands associated with $(4 - n)$Ti (n)R environments. From the obtained Ti^{4+}/R^{3+} ratios, the occupancy of octahedral sites by Ti^{4+} $(2 - x)$ and by R^{3+} (x) has been deduced with the expression

$$\frac{Ti^{4+}}{R^{3+}} = \frac{2 - x}{x} \quad (2)$$

We can see that the experimental $x^{NMR}_{R^{3+}}$ values deduced from the NMR spectra are close to the nominal $x^{Nomi}_{R^{3+}}$ ones (Table 2).

^{7}Li NMR Signal. ^{7}Li NMR ($I = {}^3/_2$) spectra of $Li_{1.2}Ti_{1.8}R_{0.2}(PO_4)_3$ samples are formed by a central line ($-{}^1/_2, {}^1/_2$ transition) and two satellite lines ($-{}^3/_2, -{}^1/_2$ and ${}^1/_2, {}^3/_2$ transitions). In ^{7}Li MAS NMR spectra, the satellite transitions are modulated by the sample rotation and it gives rise to equally spaced bands separated by the spinning rate (Figure 4). The spectra were fitted with the Bruker WINFIT program, which takes into account first-order quadrupolar interactions. From this analysis, the quadrupolar constant C_Q and the asymmetry parameter η were determined (Table 3). C_Q increases as the ionic radii of trivalent cations increases. In all cases η is equal to zero (axial symmetry).

For the samples with $R^{3+} = Al^{3+}$, Ga^{3+}, Sc^{3+}, and In^{3+}, the intensity of the central line is clearly higher than that deduced from the fitting of the NMR spectra with a single component (I_1). This suggests the presence of another component (I_2) with $C_Q \sim 0$, that has been associated with Li ions having higher mobility (Table 3). It is interesting to note that intensity of the I_2 line, between 10 and 30%, is close to the percentage of

Table 2. Chemical Shift of ^{31}P MAS NMR Components in $Li_{1.2}Ti_{1.8}R_{0.2}(PO_4)_3$ Samples; Nominal and Estimated R^{3+} Contents Are Also Included in the Table

sample	$P(OTi)_4$	$P(OTi)_3(OR)_1$	$P(OTi)_2(OR)_2$	$P(OTi)_1(OR)_3$	$x^{Nomi}_{R^{3+}}$	$x^{NMR}_{R^{3+}}$
$Ti_{1.8}Al_{0.2}$	−27.55	−26.02	−24.87	−23.32	0.20	0.21
$Ti_{1.8}Ga_{0.2}$	−27.5	−25.5	−23	−20.50	0.20	0.16
$Ti_{1.8}Sc_{0.2}$	−27.38	−25.30	−23.15	−20.85	0.20	0.18
$Ti_{1.8}In_{0.2}$	−27.14	−22.55	−19.62	−17.9	0.20	0.23

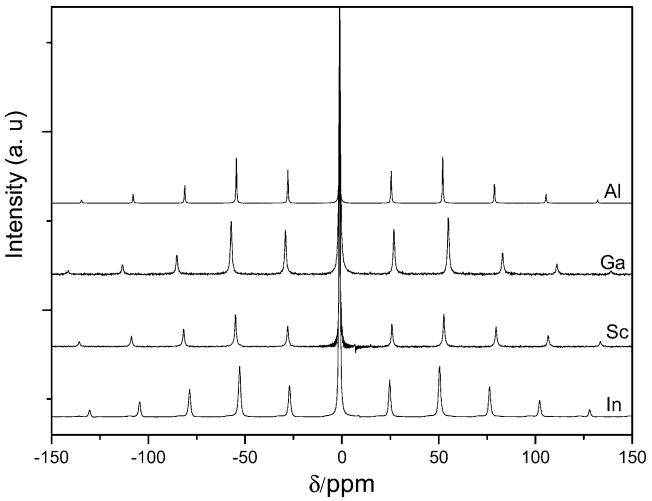

Figure 4. ^{7}Li MAS NMR spectra of $Li_{1+x}Ti^{4+}_{2-x}R^{3+}_x(PO_4)_3$ samples.

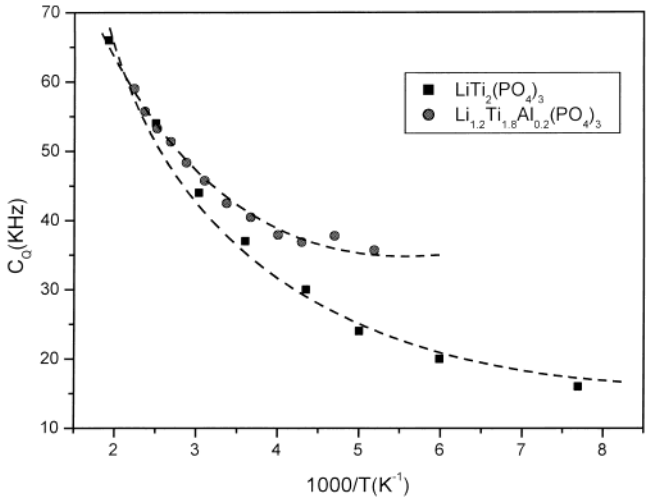

Figure 5. Temperature dependence of the quadrupole constant C_Q of $Li_{1.2}Ti_{1.8}Al_{0.2}(PO_4)_3$ and $LiTi_2(PO_4)_3$ samples.

Table 3. Quadrupole C_Q (kHz) Constants and Asymmetry Parameters η (dimensionless) as Deduced from ^{7}Li MAS NMR Spectra of $Li_{1.2}Ti_{1.8}R_{0.2}(PO_4)_3$ Series

R^{3+}	C_Q	η	I_1	I_2
Al^{3+}	44	0	85	15
Ga^{3+}	44.36	0	90	10
Sc^{3+}	52	0	70	30
In^{3+}	49	0	81	19

lithium ions incorporated into the NASICON structure according to the substitution scheme $Ti^{4+} \rightarrow R^{3+} + Li^+$.

In static ^{7}Li NMR spectra (not shown) the line-width of the central line shows values below 1000 Hz, indicating that Li mobility is important even at room temperature. Because $Li_{1.2}Ti_{1.8}Al_{0.2}(PO_4)_3$ shows the highest ionic conductivity, we have chosen this sample to analyze lithium motion mechanism. In Figure 5, we show the variation of the cuadrupole constant (C_Q) as a function of the reciprocal temperature (1000/T) for the Al sample and the undoped one. For the Al sample an important broadening of the satellite transitions makes difficult the determination of C_Q below 175 K. This

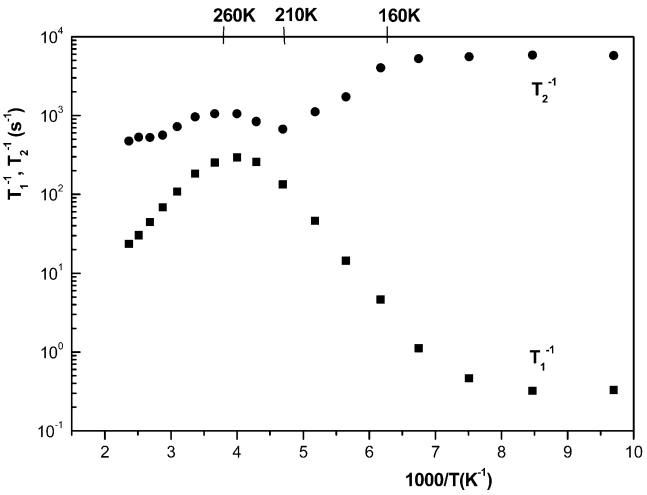

Figure 6. Temperature dependence of the ^{7}Li NMR spin−lattice ($1/T_1$) and spin−spin ($1/T_2$) relaxation rates of the $Li_{1.2}Ti_{1.8}Al_{0.2}(PO_4)_3$ sample. Experiments were carried out at 11 MHz.

broadening decreases as temperature increases, and it allows determination of C_Q. Below 250 K, the C_Q is almost constant (35 kHz) in $Li_{1.2}Ti_{1.8}Al_{0.2}(PO_4)_3$ sample, but above this temperature C_Q increases toward values measured in the $LiTi_2(PO_4)_3$ sample. This observation goes parallel to the detection of the second central component I_2, ascribed to mobile lithium species. According to this fact, two species with different mobility coexist in the Al sample.

T_2^{-1} (spin−spin) and T_1^{-1} (spin−lattice) relaxation rates, deduced from the central transition, are plotted vs reciprocal temperature in Figure 6. In the 100−160 K range, T_2^{-1} remains constant indicating the absence of lithium mobility. In this case, the nearly constant T_1^{-1} values are probably due to the nuclear relaxation induced by paramagnetic impurities. When the temperature increases ($160 < T < 210$ K), lithium mobility increases producing the narrowing of the ^{7}Li NMR central line. At the same time, T_1^{-1} increases and T_2^{-1} decreases, the latter reaching a minimum at 210 K. At 260 K, a maximum of T_1^{-1} and T_2^{-1} is detected. At increasing temperature, T_1^{-1} and T_2^{-1} decrease again indicating the onset of more extended Li motions. Above 350 K, T_2^{-1} remains constant because the contribution of the external magnetic field inhomogenities become more important than T_2^{-1} values.

Conductivity

The angular frequency dependence of the conductivity for the Ga sample is shown in Figure 7 (top). These plots are typical for all the other samples. At 280 K, three features are observed: (i) an ill-defined dispersive regime below 10^2 s^{-1}; (ii) a plateau in the frequency range 10^2−10^4 s^{-1}, followed by a dispersive regime at around 10^6 s^{-1}; and (iii) an ill-defined plateau at about 10^7 s^{-1}, followed again by a dispersive regime. At lower temperatures, 150 and 200 K, the three features are shifted toward lower frequencies. The features (i), (ii), and (iii) correspond to the spike, the low-frequency arc, and the high-frequency arc, respectively, that are observed in the impedance plots (not shown). The

(20) París, M. A.; Sanz, J. *Phys. Rev. B* **1997**, *55*, 14270−14278.
(21) Losilla, E. R.; Aranda, M. A. G.; Bruque, S.; París, M. A.; Sanz, J.; Campo, J.; West, A. R. *Chem. Mater.* **2000**, *12*, 2134−2142.

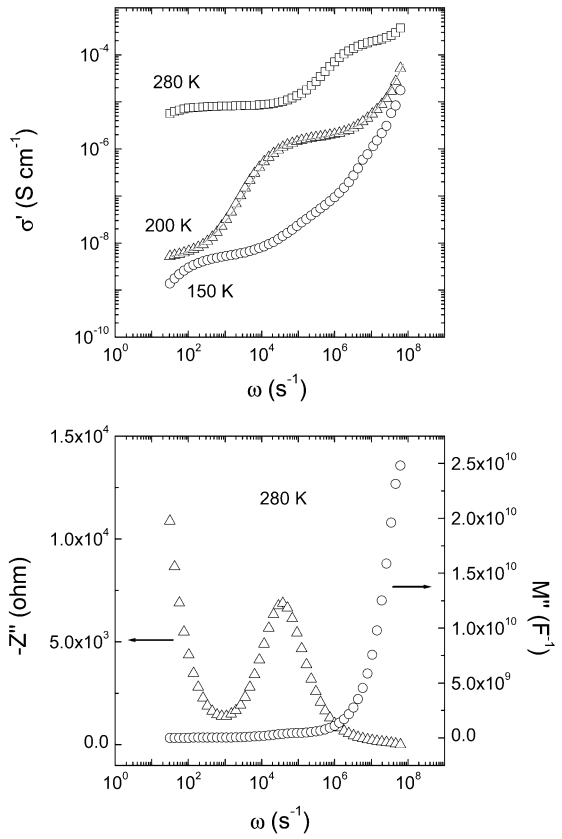

Figure 7. Top: real conductivity versus angular frequency at indicated temperatures for the Ga sample. The solid line corresponds to the best fitting of the data obtained at 200 K. Bottom: imaginary impedance ($-Z''$) and imaginary modulus (M'') versus angular frequency for the same sample.

capacitance associated with the high-frequency arc, and hence with the high-frequency plateau, is of 8 pF. The capacitance associated with the low-frequency arc, and hence with the low-frequency plateau, is of 1 nF. The approximate capacitance of the used cell is of 2 pF. In accordance with the capacitances found, the features (ii) and (iii) are associated with the grain boundary response and the grain interior one, respectively,[22,23] i.e., with the motion of Li^+ through boundary of adjacent grains and within the grains, respectively.

The three responses mentioned are also observed in the $-Z''(\omega)$ and $M''(\omega)$ plots (Figure 7, bottom). In the former (open triangles) the ill-defined peak at low frequencies and the peak at intermediate frequencies correspond to the electrode and grain-boundary responses, respectively. The peak due to the grain interior response is not observed because of the low intensity of this peak compared to the two others. However, the grain interior response gives rise to the peak developed at high frequencies in the $M''(\omega)$ plot (open circles). In this case the grain boundary and electrode responses cannot be observed because their capacitances are much higher than that of the grain interior response.

The experimental $\sigma'(\omega)$ data (Figure 7, top) have been fitted with the expression

$$\sigma^* = (1/\sigma_1^* + 1/\sigma_2^*)^{-1} \qquad (3)$$

where the σ^* accounts for the overall complex conductivity and σ_1^* and σ_2^* account for grain interior and grain boundary contributions, respectively. When the electrode response at low frequencies is important, an additional $1/\sigma_3^*$ contribution was included in eq 3. To reproduce the experimental conductivity, σ_1^* and σ_2^* were assumed to adopt the form $\sigma_{dc} + B(i\omega)^n$, where σ_{dc} (dc conductivity) accounts for the plateau and $B(i\omega)^n$ is for the dispersive regime.[24] In the case of σ_3^* only a dispersive regime of type $A\omega^p$ was taken into account. As an example, the fitting obtained at 200 K (solid line) is shown in Figure 7 (top). By this way, we have estimated the dc conductivity for the grain interior and for the grain boundary, the latter being in most cases almost coincident with the overall dc conductivity of the pellet. The grain interior dc conductivity and the overall dc conductivity obtained at 250 K for the Al, Ga, Sc, and In samples are outlined in Table 4.

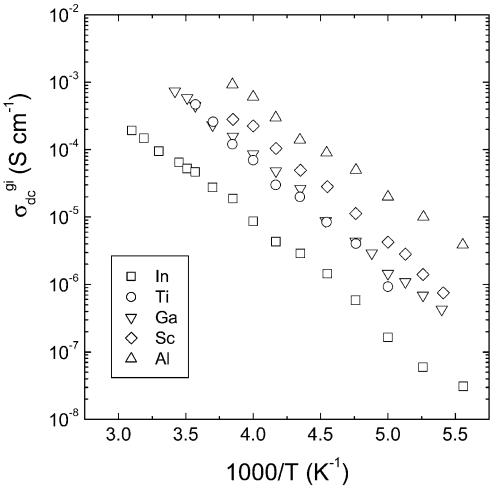

Figure 8. Grain interior dc conductivity for the $Li_{1+x}Ti^{4+}_{2-x}R^{3+}_x(PO_4)_3$ series versus reciprocal temperature (1000/T). The conductivity measured on $LiTi_2(PO_4)_3$ is included as a reference.

Table 4. Activation Energies, Pre-Exponential Factors, and Conductivities at 250 K of the $Li_{1.2}Ti^{4+}_{1.8}R^{3+}_{0.2}(PO_4)_3$ Series (σ^{gi} and σ^{ov} Stand for Grain Interior and Overall Conductivities)

R	E (eV)	σ_0 (S cm^{-1})	σ^{gi}_{250K} (S cm^{-1})	σ^{ov}_{250K} (S cm^{-1})
Al	0.28 ± 0.01	280 ± 60	5.5×10^{-4}	2.5×10^{-6}
Ga	0.33 ± 0.01	400 ± 70	8.3×10^{-5}	6.6×10^{-7}
Sc	0.33 ± 0.01	1100 ± 500	1.9×10^{-4}	1.4×10^{-6}
In	0.32 ± 0.01	20 ± 5	7.9×10^{-6}	1.5×10^{-6}

Variation of the grain interior dc conductivity ($\sigma_{dc}{}^{gi}$) vs reciprocal temperature (1000/T) is shown for all the analyzed samples in Figure 8. The experimental data obtained below 300 K are fitted to the Arrhenius expression

$$\sigma_{dc}{}^{gi} = \sigma_0 \exp(-E/kT) \qquad (4)$$

where σ_0 is a preexponential factor, E is the activation energy, k is the Boltzmann constant, and T is the absolute temperature. Values of σ_0 and E deduced from the fittings are outlined in Table 4. The activation energy is quite similar for the Ga, Sc, and In samples

(22) Macdonald, J. R. *Impedance Spectroscopy. Emphasizing Solid Materials and Systems*; John Wiley & Sons: New York, 1987.
(23) Irvine, J. T. S.; Sinclair, D. C.; West, A. R. *Adv. Mater.* **1990**, *2*−*3*, 132.
(24) Jonscher, A. K. In *Dielectric Relaxation in Solids*; Chelsea Dielectric Press: London, 1983.

($E \approx 0.33$ eV), but σ_0 is different. The Al^{3+} sample displays the lowest activation energy ($E = 0.28$ eV).

Discussion

The overall conductivity of the pellets, measured at 250 K (Table 4), is in general much lower (at least 2 orders of magnitude) than the grain interior conductivity. Only in the In-pellet, the overall conductivity similar to that of the grain interior, pointing out that the pellet has been well-sintered. These results provide evidence that the overall conductivity is, in general, dominated by the grain boundary contribution. The same effect was reported by Aono et al. in samples with similar compositions.[13]

The activation energy for the grain interior conductivity of most samples is similar (0.33 eV) and lower than that of the undoped sample. The lowest activation energy was found for the Al sample (0.28 eV); this result is in agreement with that reported by Aono et al.[25] No correlation between activation energy and ionic radii of the trivalent cations has been found. The Al sample displays the highest conductivity at 250 K (5.5×10^{-4} Scm^{-1}) and the lowest activation energy (0.28 eV). In the Ga, Sc, and In samples, in which the cation size increases, the conductivity decreases from 2×10^{-4} to 8×10^{-6} Scm^{-1} and the activation energy remains constant.

Deconvolution of ^{31}P NMR spectra has allowed the determination of the octahedral cation content for the $Li_{1.2}Ti_{1.8}R_{0.2}(PO_4)_3$ compounds (see Table 2). It is observed that the amount of trivalent cations incorporated into the NASICON structure increases in the sense Ga < Sc < Al < In. With the exception of the In sample, this trend is parallel to the increase in grain interior conductivity measured. For the In sample, in which the concentration of mobile species is the highest but the conductivity is the lowest, other structures with lower conductivity could be formed;[15−16] however, in our case no extra peaks have been detected in XRD patterns. The above observations suggest that compositional rather than geometrical factors are controlling the lithium mobility of these compounds. Indeed, the highest grain interior conductivity is obtained in the $Li_{1.2}Ti_{1.8}^{4+}R_{0.2}^{3+}(PO_4)_3$ sample, where R^{3+} is the smallest cation.

Lithium Structural Sites. Structural sites occupied by lithium can be deduced from the analysis of the experimental second moment ($\Delta\varpi^2$) of the ^7Li NMR signal recorded in static conditions at low temperature (absence of lithium motion). For that, experimental $\Delta\varpi^2$ values have been compared with those calculated with the expression[26]

$$\Delta\varpi^2 = \frac{3}{5}\gamma_I^4\hbar^2 I(I+1)\sum_k \frac{1}{r_{jk}^6} + \frac{4}{15}\gamma_I^2\gamma_S^2\hbar^2 S(S+1)\sum_k \frac{1}{r_{jk}^6} \quad (5)$$

where the first term accounts for dipolar interactions between like spins and the second one accounts for interactions between unlike spins. γ_I and γ_S are the gyromagnetic ratios of I and S spins and r_{jk} is the distance between interacting spins.

Below 160 K, the line width of the ^7Li NMR central line ($\propto T_2^{-1}$) remains constant (Figure 6) indicating the absence of lithium motion. In the Al sample analyzed, $\Delta\varpi^2$ has been calculated for Li placed at the M_2 site ($\sim$0.33 G^2), at the midway $M_{1/2}$ site ($\sim$0.24 G^2), and at the M_1 site ($\sim$0.13 G^2). The latter is close to the experimental value ($\sim$0.14 G^2) measured at 160 K, confirming the preferential occupancy of M_1 sites by lithium. In these sites, the contribution to $\Delta\varpi^2$ of Li−P interaction ($\sim$0.09 G^2) is higher than that of the Li−Li interaction ($\sim$0.04 G^2) and the contribution of Li−Ti interaction is negligible. In agreement with this analysis, the quadrupole C_Q constant calculated for M_1 sites is similar to that deduced from NMR spectra, and the asymmetry parameter deduced ($\eta = 0$) is characteristic of sites with the axial symmetry.[27]

Lithium Mobility. In this section, lithium motion mechanisms have been analyzed in the $Li_{1.2}Ti_{1.8}Al_{0.2}(PO_4)_3$ sample because it displays the highest grain interior conductivity and the lowest activation energy. When the sample is heated above 160 K (Figure 6), the ^7Li NMR line width (T_2^{-1}) decreases, indicating that mobility of lithium increases (spectral line narrowing). The increase in Li mobility is also responsible for the increase of T_1^{-1} observed above 160 K and the maximum detected at 260 K in the T_1^{-1} plot. In general, the temperature dependence of T_1^{-1} and T_2^{-1} can be described with the modified BPP expressions[28−29]

$$T_1^{-1} = C\left[\frac{\tau_c}{1+(\omega\tau_c)^{1+\beta}} + \frac{4\tau_c}{1+(2\omega\tau_c)^{1+\beta}}\right] \quad (6)$$

$$T_2^{-1} = \frac{1}{2}C\left[3/\tau_c + \frac{5\tau_c}{1+(\omega\tau_c)^{1+\beta}} + \frac{2\tau_c}{1+(2\omega\tau_c)^{1+\beta}}\right] \quad (7)$$

where C depends on the magnetic interaction that causes the nuclear relaxation, τ_c is the residence time at the structural sites, and β is a constant that takes into account correlation effects on the Li motion. The temperature dependence of τ_c is given by

$$\tau_c = \tau_{c0}\exp(E_M/kT) \quad (8)$$

where E_M is the long-range activation energy for the lithium motion and k is the Boltzmann constant.

The C constant, deduced from the fitting of the T_1^{-1} plot, was $C \approx 5 \times 10^9$ s^{-2}. If the Li relaxation was produced by fluctuations on quadrupole interactions at sites occupied by lithium, C_Q values can be calculated with the expression[27]

$$C \approx \left(\frac{2\pi^2}{5}\right)\left(1+\frac{\eta^2}{3}\right)C_Q^2 \quad (9)$$

The C_Q deduced ($\sim$40 kHz) is close to the value deduced from ^7Li NMR spectrum at 200 K, confirming that quadrupolar interactions are responsible for Li

(25) Aono, H.; Sugimoto, E.; Sadaoka, Y.; Imanaka, N.; Adachi, G.-Y. *Chem. Lett.* **1990**, *10*, 1825−1828.
(26) Van Vleck, J. H. *Phys. Rev.* **1948**, *74*, 1168.
(27) París, M. A.; Martinez-Juárez, A.; Rojo, J. M.; Sanz, J. *J. Phys. Condens. Matter* **1996**, *8*, 5355−5366.
(28) Grüne, M.; Müller-Warmuth, W. *Phys. Chem.* **1991**, *95*, 1068−1071.
(29) Kanert, O.; Küchler, R.; Ngai, K. L.; Jain, H. *Phys. Rev. B* **1994**, *49*, 76−82.

relaxation. If dipolar interactions were the dominant contributions, the expected C constant ($C \approx \Delta\varpi^2$) should be 2 orders of magnitude lower.

At the T_1^{-1} maximum, the residence time of lithium ions at the occupied sites is $\tau_c \approx \omega_0^{-1} \approx 1.5 \times 10^{-8}$ s ($\omega_0\tau = 1$), indicating that Li mobility is very high at 260 K. In the 160−260 K range, the activation energy deduced from the linear fitting of T_1^{-1} is $E_m = 0.19$ eV. This value is considerably lower than that deduced in the undoped $LiTi_2(PO_4)_3$ sample ($E_m = 0.45$ eV). This fact has been interpreted by assuming that the additional Li incorporated in $Li_{1.2}Ti_{1.8}Al_{0.2}(PO_4)_3$ increases electrostatic Li−Li interactions and destabilizes the occupancy of M_1 sites, decreasing the activation energy. On the other hand, these interactions increase the amount of vacant M_1 sites and favor long-range Li motion along the conduction pathways. Because the activation energy deduced from conductivity ($E_M = 0.28$ eV) is considerably higher than that deduced from NMR ($E_m = 0.19$ eV), the motion of Li ions must be correlated in In $Li_{1.2}Ti_{1.8}Al_{0.2}(PO_4)_3$. Taking into account Ngai's equation[30] $E_m = \beta E_M$, which relates the activation energy of short- (E_m) and long-range (E_M) motions, deduced from NMR and conductivity respectively, the calculated correlation factor is $\beta = E_m/E_M \approx 0.7$.

In general, T_2^{-1} decreases in a monotonic way as the temperature increases; however, in our case T_2^{-1} values display a maximum at 260 K. The increase detected between 210 and 260 K has been ascribed to an increase of dipolar interactions. In this sample, dipolar Li−P interactions calculated at $M_{1/2}$ sites are higher than those at M_1 sites. From this fact, we have assumed that a progressive occupancy of $M_{1/2}$ sites at the expense of that of M_1 sites is produced at increasing temperatures. The complex evolution of T_2^{-1} versus $1000/T$ coincides with the increase of C_Q detected at increasing temperature (Figures 5 and 6). This trend, which cannot be explained by hopping of Li^+ ions between equivalent sites, indicates again that lithium occupies, besides the M_1 site, other sites with lower symmetry (sites $M_{1/2}$) at increasing temperatures.

If we assume that lithium exchanges between M_1 and $M_{1/2}$ sites, the observed C_Q evolution could be calculated with the expression[31]

$$C_Q = \frac{C_Q{}^1 P_1 + C_Q{}^2 3P_2}{P_1 + 3P_2} \qquad (10)$$

where $C_Q{}^1$ and $C_Q{}^2$ are the quadrupolar constants at the M_1 and $M_{1/2}$ sites, and P_1 and P_2 are the occupation probabilities of those sites, respectively. The factor 3 takes into account the multiplicity of the $M_{1/2}$ sites with respect to the M_1 sites. The experimental C_Q values are well-reproduced by assuming C_Q values deduced previously for the M_1 and $M_{1/2}$ sites, 45 and 180 kHz, respectively.[31−32] A fast exchange process between both sites explains that only one signal with axial symmetry ($\eta = 0$) is detected.

The T_1^{-1} plot shows in the temperature range 213−300 K a broad maximum that is not possible to be fitted on the basis of a single relaxation mechanism. From this fact and according to observations obtained in C_Q and T_2^{-1} analysis, we have assumed the presence of two relaxations processes associated with local and extended motions of lithium. In the former case, mobile Li ions have a high probability to come back to starting M_1 positions; however, in the latter case local motions of Li give rise to long-range motions with simultaneous occupation of M_1 and $M_{1/2}$ sites. In this analysis, observed T_1^{-1} and T_2^{-1} values have been described with the expressions

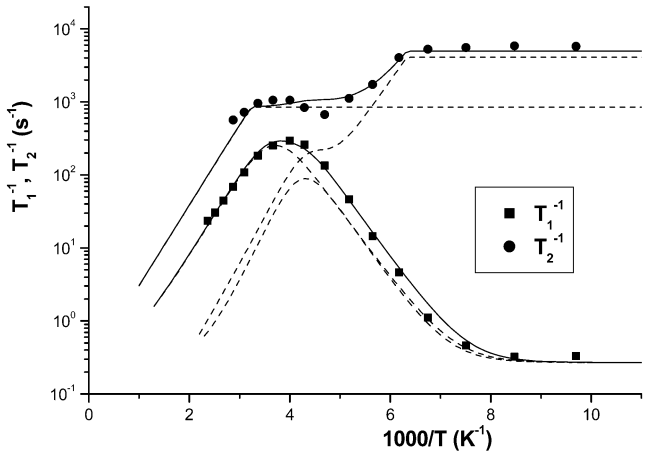

Figure 9. Fitting of the ^{7}Li NMR spin−lattice ($1/T_1$) and spin−spin ($1/T_2$) relaxation rates of the $Li_{1.2}Ti_{1.8}Al_{0.2}(PO_4)_3$ compound with two relaxation mechanisms. In this analysis, two modified BBP expressions were used (see text).

$$\frac{1}{T_1} = \frac{1}{T_1{}^{LT}} + \frac{1}{T_1{}^{HT}} + \frac{1}{T_1{}^{PAR}} \qquad (11)$$

$$\frac{1}{T_2} = \frac{1}{T_2{}^{LT}} + \frac{1}{T_2{}^{HT}} + \Delta\omega \qquad (12)$$

where $(T_1{}^{HT})^{-1}$, $(T_2{}^{HT})^{-1}$ and $(T_1{}^{LT})^{-1}$, $(T_2{}^{LT})^{-1}$ stand for local and extended motions of lithium, and $(T_1{}^{PAR})^{-1}$ and $\Delta\omega$ correspond to contributions of the paramagnetic impurities and the magnetic field inhomogenity, respectively. At low temperatures the $(T_1{}^{PAR})^{-1}$ contribution is preponderant due to the absence of lithium motion. At high temperatures, the contribution of field inhomogenity, $\Delta\omega$, becomes more important than T_2^{-1} values.

In the analysis of T_1^{-1} plots, we have assumed two relaxation mechanisms with the same activation energy, $E_m = 0.19$ eV, but different β. This assumption produces different E_M values for two lithium motion stages ($E_M = 0.29$ and 0.22 eV). With these assumptions a good fitting of T_1^{-1} and T_2^{-1} plots was obtained (Figure 9). The decrease observed on T_2^{-1} above 300 K has been associated with an increase of lithium mobility that reduces the residence time at M_1 and $M_{1/2}$ sites. From the temperature dependence of T_1^{-1} values was deduced an activation energy $E_M = 0.22$ eV, corresponding to long-range motions of lithium in the temperature range 300−450 K. In the relaxation model assumed, the correlation time extrapolated at high temperature (τ_{c0}) can be deduced with eq 8. In the case of local motions $\tau_{c01} \approx 10^{-14}$ s and in the case of extended motions $\tau_{c02} \approx 10^{-12}$ s.

(30) Ngai, K. L. *Phys. Rev. B* **1993**, *48*, 13481−13485.
(31) París, M. A.; Martínez-Juárez, A.; Iglesias, J. E.; Rojo, J. M.; Sanz, J. *Chem. Mater.* **1997**, *9*, 1430−1436.
(32) París, M. A.; Sanz, J. *Phys. Rev. B* **2000**, *62* (2), 810−817.

If we compare the activation energy corresponding to long-range motions deduced from impedance spectroscopy at low temperature ($T < 260$ K) and that deduced from the high-temperature branch of T_1^{-1} NMR curve ($T > 300$ K), it can be concluded that the activation energy E_M decreases from 0.29 to 0.22 eV as temperature increases. The observed decrease of E_M could be ascribed to a decrease of the activation energy E_m or to an increase of the β factor. Taking into account that structural modifications are not produced at increasing temperature in the rhombohedral phase, the observed decrease on E_M probably corresponds to the decrease in Li-motion correlations (β increment).To ascertain this point the grain interior conductivity should be measured at higher frequencies and temperatures.

Conclusion

Composition and lithium mobility of $Li_{1+x}Ti^{4+}_{2-x}R^{3+}_x(PO_4)_3$ compounds ($x = 0.2$ and $R^{3+} = Al^{3+}$, Ga^{3+}, Sc^{3+}, and In^{3+}) have been analyzed with XRD, NMR, and impedance spectroscopy. In the analyzed samples, most of the trivalent cations are incorporated into the NASICON structure, increasing the amount of mobile lithium ions. The preferential occupancy of M_1 sites by lithium was deduced from the analysis of ^{7}Li MAS NMR spectra.

From the frequency dependence of the conductivity, the grain interior and grain boundary contributions were determined. In the case of $Li_{1.2}Ti_{1.8}Al_{0.2}(PO_4)_3$, which displays the highest grain interior conductivity, the hopping mechanism of lithium has been analyzed by ^{7}Li NMR spectroscopy. Two different regimes, associated with local and extended motions of Li ions, were deduced from the temperature dependence of T_1^{-1} and T_2^{-1}. From the dependence of C_Q versus temperature, the partial occupancy of midway $M_{1/2}$ sites at the expense of those of M_1 was deduced at increasing temperatures. An exchange process between M_1 and $M_{1/2}$ sites appears when residence times at structural sites decrease below 10^{-8} s. A considerable decrease in the activation energy is observed as extended motions are established; this decrease has been ascribed to the increment of the correlation factor β. The observed increment indicates a decrease of correlated motions at increasing temperatures.

Acknowledgment. Financial support provided by the Spanish CICYT, projects MAT2001-0562 and MAT2001 373-CO4, is acknowledged. K. Arbi and M. G. Lazarraga thank the Spanish Ministry of Science and Technology and Ministry of Education, Culture and Sport, respectively for the fellowships received.

CM030422I